JOURNAL OF PROPULSION AND POWER
Vol. 24, No. 5, September–October 2008

Elevated Pressure Thermal Experiments and Modeling Studies on the Water-Gas Shift Reaction

Brad Culbertson,* Raghu Sivaramakrishnan,† and Kenneth Brezinsky‡
University of Illinois at Chicago, Chicago, Illinois 60607

DOI: 10.2514/1.31897

The water-gas shift reaction influences the chemistry between the postcombustion gases of a rocket and the rocket's graphite nozzle. The rocket's operating pressures (70–600 atm) exceed those for existing water-gas shift reaction data, and further study of the chemistry under similar conditions is essential for optimum rocket design. To investigate chemical kinetic effects at the pertinent pressure and temperature regime, experiments were performed using the University of Illinois at Chicago high-pressure shock-tube facility with experimental temperatures ranging from 1200–2100 K and pressures ranging from 194–490 atm with reaction times averaging 1.17 ms. Initial mole fractions of H_2O and CO were varied from 115–983 ppm (0.0002–0.003 mol/L). The experimental data have been compared with predictions from a comprehensive model for synthesis gas ($CO/H_2/CO_2$) combustion and a reduced four-step model with the chemistry relevant to the water-gas shift reaction. The rate coefficients at our elevated pressure and temperature conditions were found to be pressure independent when compared with prior lower temperature 1 atm measurements.

Nomenclature

A = Arrhenius preexponential constant
E_a = activation energy
k = reaction rate coefficient
n = non-Arrhenius temperature coefficient
r = reaction rate
T_5 = reflected shock temperature

Introduction

THE water-gas shift reaction (WGSR) is critical to understanding the overall chemistry that takes place when combustion exhaust interacts with the graphitic nozzle surface in rockets. Essentially, two reactions have been postulated by Kuo and Keswani [1] to have a detrimental influence on the graphitic nozzles, with the WGSR becoming important when H_2O is present.

$$C_{(s)} + CO_2 = 2CO \tag{1}$$

$$C_{(s)} + H_2O = CO + H_2 \tag{2}$$

$$CO + H_2O = CO_2 + H_2 (WGSR) \tag{3}$$

Reactions (1) and (2) represent the key heterogeneous reactions between the graphitic rocket nozzle surface $C_{(s)}$ and the most abundant postcombustion gases, viz., CO_2 and H_2O that erode the nozzle. Reactions (1) and (2) form the subject of an ongoing experimental and modeling study in our high-pressure shock-tube facility (HPST). However, to better understand the contributions to nozzle erosion via reactions (1) and (2), the key homogeneous reaction, the WGSR needs to be well characterized under a high-pressure, high-temperature environment and this forms the subject of the present article.

The WGSR, both the forward and reverse reaction, has been studied in prior work [2–4], mainly focusing on synthetic-gas combustion [2,3] or catalysis for fuel cell research [4]. Much of the catalytic studies on the WGSR, as well as its applications in Fischer-Tropsch synthesis, have been summarized in a recent detailed review article by Van der Laan and Beenackers [5]. None of these prior studies experimented in the high-pressure and high-temperature environment to which the rocket nozzle is exposed (70–600 atm and 2000–3500 K). The most recent studies by Bustamante et al. [2,3] showed a decrease in the overall reaction rate simply by raising the pressure from 1 to 16 atm. Bustamante et al.'s [3] 16 atm experiments used a quartz reactor for studying the WGSR at temperatures from 1030–1174 K. One key factor to note about the Bustamante et al. [2,3] studies is that their experiments were thermally initiated (noncatalytic).

Before the Bustamante [3] study, the only noncatalytic investigation on the WGSR in the literature appears to be that of Graven and Long [6]. Before Graven and Long, several other studies by Hadman et al. [7], Bradford [8], and Long and Sykes [9] focused on the WGSR as part of their studies into CO oxidation in the presence of water. However, the Graven and Long [6] experiments were the only direct and detailed study.

Graven and Long [6] studied the WGSR in both directions using a quartz vessel at temperatures from 875–1050°C and 0.1 MPa at reaction times of 0.5 s. Their experiments were used to derive the order of the reaction with respect to CO and H_2O, as well as overall rate parameters and the equilibrium constant for the WGSR. The recent experiments of Bustamante et al. [3] are consistent with the Graven and Long [6] experiments with regard to the order of the reaction, despite differences in the derived rate parameters. Furthermore, the Bustamante et al. [3] studies match the Graven and Long [6] experiments at low pressures (0.1 MPa) but show deviations at higher pressures of 1.6 MPa.

With an operating pressure of over 300 atm, the chemistry inside the rocket nozzle may have considerable effects from the high pressure. With the recent experiments of Bustamante et al. [2,3] appearing to indicate a pressure dependence, the WGSR may play a dominant role at the elevated pressure and temperature conditions experienced by the rocket nozzle, motivating the current

Received 1 May 2007; revision received 8 May 2008; accepted for publication 15 May 2008.

*Graduate Student, Department of Mechanical and Industrial Engineering, 2039, Engineering Research Facility, Mail Code 251, 842 West Taylor Street.
†Research Scientist, Department of Mechanical and Industrial Engineering, 2039, Engineering Research Facility, Mail Code 251, 842 West Taylor Street.
‡Professor, Department of Mechanical and Industrial Engineering, 2039, Engineering Research Facility, Mail Code 251, 842 West Taylor Street.

experimental studies at elevated pressures and temperatures in the University of Illinois at Chicago HPST.

Experimental

High-pressure shock-tube experiments were performed at the HPST facility. A detailed description of the shock tube and its operation can be obtained from prior studies [10,11]. The shock tube is a well characterized experimental setup [11,12] and has been used recently in related work on CO oxidation at similar high-pressure, high-temperature conditions [13]. The current experiments were performed behind the reflected shock wave using a driver section [length of 1.52 m (60 in.) with a 5.08 cm (2 in.) bore] separated from the driven section [length of 2.57 m (101 in.) with a 2.54 cm (1 in.) bore] by means of prescored brass and aluminum diaphragms. Reaction pressures ranged from 194–490 atm, temperatures ranged from 1200–2100 K, and reaction times averaged 1.17 ms. The calculations of the temperatures and reaction times are described in previous publications [11,12]. Zero grade purity (99.998%) helium supplied by Airgas was used as the driver gas to burst the diaphragms and generate the shock wave. The test gas mixtures were prepared in a heated 50l stand-alone mixture vessel and allowed to stand overnight (homogenize) before use. Mixtures contained varying quantities of CO, H_2O, H_2, and Ne with Ar as balance. Table 1 lists the dilute initial mole fractions of reacting species. Dilute mixtures were used to ensure the experimental temperatures were isothermal and not influenced by the heat of reaction [11]. Advanced Specialty Gases supplied the CO (99.999%), and Airgas supplied the ultrahigh purity H_2 (99.999%) as well as the ultrahigh purity Ar and research grade 5.0 Ne. The gases were used as supplied, with the only exception being the bath gas argon which was passed through a Matheson Oxisorb filter to remove trace amounts of oxygen. Distilled H_2O in a glass bulb was admitted into the heated mixture vessel after several cycles of a freezing and thawing process, to remove any air in the bulb, with no traceable impurities found upon gas chromatography/mass spectrometry (GC/MS) analysis.

The diagnostic technique used in these experiments involves offline analysis of the quenched postshock gases, sampled from the end wall of the shock tube, using GC/MS. Two Hewlett-Packard (HP) 6890 GC's, one equipped with an HP-5973 MS and a VALCO helium pulse discharge photoionization detector, and the other with standard HP flame ionization/thermal conductivity detectors, were used to perform the analysis for the stable species from the high-pressure experiments. Along with the two reactants CO and H_2O, the primary products CO_2 and H_2 were also detected using the diagnostic setup. The detectors were calibrated using reference standards and care was taken to ensure accuracy within 10% for the species measurements made in these current experiments.

Results

A variety of experiments were performed with the preliminary studies using initial mole fractions of approximately 1000 ppm for both CO and H_2O at postshock pressures of 307 atm. The species CO and CO_2 are plotted in Fig. 1 as a function of calibrated shock temperature; the H_2O and H_2 profiles matched the CO and CO_2 profiles, respectively, but were left out of the following figures. The CO begins to react at 1500 K and 25% of the initial CO is gone at the highest temperatures in these experiments (1900 K). CO_2 correspondingly begins to form at 1500 K and increases up to amounts equal to the CO that was consumed.

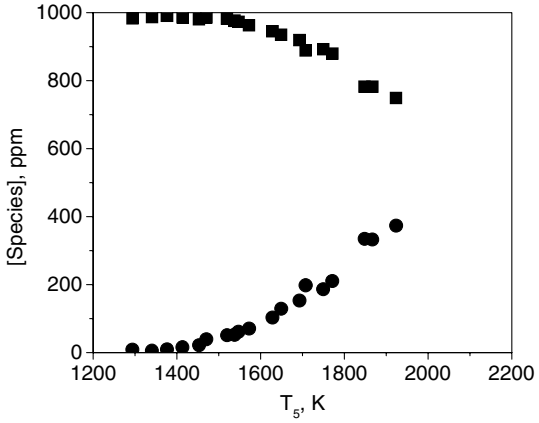

Fig. 1 307 atm, 1000 ppm: ■ CO experiment, ● CO_2 experiment.

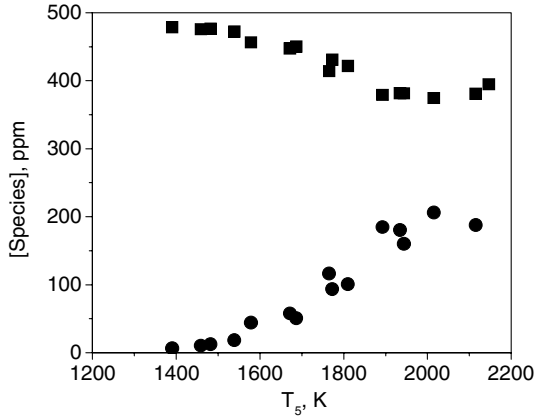

Fig. 2 299 atm, 475 ppm: ■ CO experiment, ● CO_2 experiment.

Figure 2 depicts the experimental data using 475 ppm of each reactant at postshock pressures of 299 atm. The trends are similar to Fig. 1 with the higher mole fraction mixture, with the only exception being that at $T > 1900$ K, the CO profile appears to attain a plateau with no further reaction. Corresponding to the observed CO profile, the CO_2 mole fraction also attains a plateau at $T > 1900$ K. Figure 3 shows the data using very dilute mixtures of 120.7 ppm of each reactant, and trends similar to Fig. 2 are observed with the only difference being the onset of reaction, which appears to be delayed to 1600 K and the CO plateau occurring at lower temperatures of 1850 K. Again, the CO_2 formation mirrors the observed CO profile. Figures 1–3 depict experiments at pressures of approximately 300 atm.

Two sets of experiments were also performed at higher postshock pressures of approximately 500 atm using dilute reagents mixtures with equivalent amounts 237.5 and 115 ppm of the reactants CO and H_2O. Figure 4 shows the CO and CO_2 profiles for the 237.5 ppm experiments and is similar to the lower pressure 300 atm

Table 1 Initial compositions of test mixtures

Set	CO, ppm	H_2O, ppm	H_2, ppm	Pressure, atm[a]	Temperature, K	Reaction time, s[a]
1	983	900	——	307	1200–2000	1.14×10^{-3}
2	475	475	——	299	1400–2100	1.15×10^{-3}
3	120.7	120.7	——	296	1300–2000	1.20×10^{-3}
4	237.5	237.5	——	490	1300–2100	1.14×10^{-3}
5	115	115	——	475	1300–2100	1.21×10^{-3}
6	214	270	320	290	1400–2100	1.09×10^{-3}
7	203	270	311	194	1200–2000	1.27×10^{-3}

[a]Pressures refer to average nominal pressures. For exact pressures and reaction times refer to supplementary information.

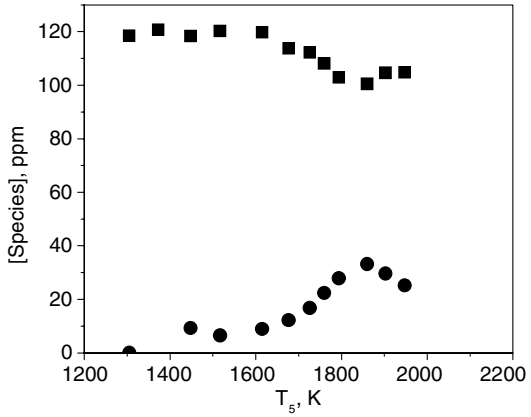

Fig. 3 296 atm, 120.7 ppm: ■ CO experiment, ● CO_2 experiment.

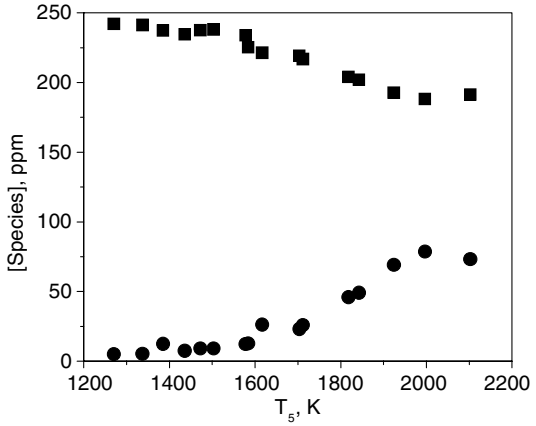

Fig. 4 490 atm, 237.5 ppm: ■ CO experiment, ● CO_2 experiment.

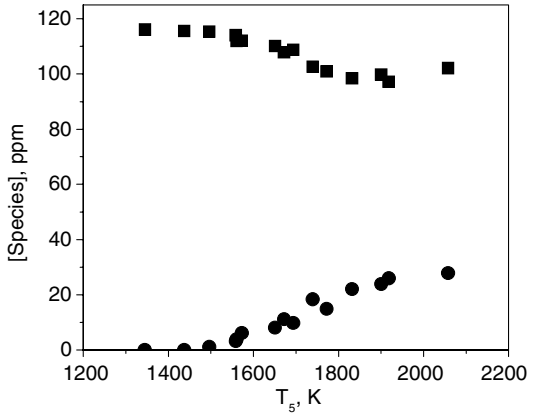

Fig. 5 475 atm, 115 ppm: ■ CO experiment, ● CO_2 experiment.

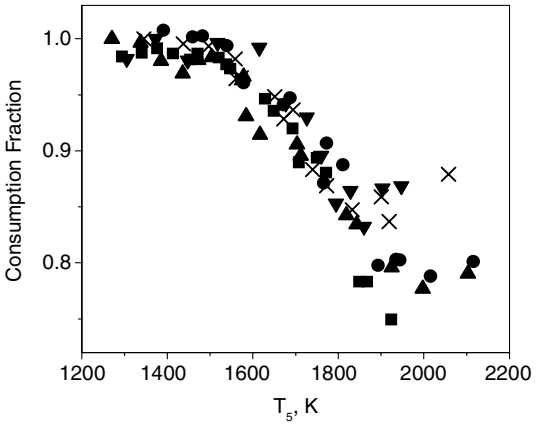

Fig. 6 Normalized CO: ■ 307 atm, 1000 ppm; ● 299 atm, 475 ppm; ▲ 490 atm, 237.5 ppm; ▼ 296 atm, 120.7 ppm; X 475 atm, 115 ppm.

experiments, particularly the 299 atm, 475 ppm experiments in Fig. 2 (these experiments have the same initial CO and H_2O concentrations as the 490 atm, 237.5 ppm mix) with CO beginning to react at 1500 K and plateauing at the highest temperatures around 1900 K. Figure 5 shows data obtained from 475 atm shocks with 115 ppm initial mole fractions of CO and H_2O. CO again begins to react at temperatures above 1500 K and reaches a plateau at 1850 K and most closely mimics the trends seen for the experiments with the most dilute reagent mixtures (the 296 atm, 120.7 ppm data depicted in Fig. 3).

The CO profiles for all the experimental sets are summarized in Fig. 6, which plots the consumption fractions as a function of reaction temperature. The maximum normalized CO reaction occurred in the 307 atm, 1000 ppm experiments with 25% reacting. These experiments have the largest initial reactant concentrations. The extent of reaction decreased with decreasing CO and H_2O concentrations, with only 15% of the CO reacting in the most dilute 120.7 ppm experiments at 296 atm. The experiments depicted in Figs. 1–5 and summarized in Fig. 6 represent the first such thermal studies into the WGSR at elevated pressure and temperature conditions. We have probed this WGSR system further by studying the effects of doping with H_2 and observing the trends on the reactivity of CO with the dopant.

These experiments were performed to test the observations of Graven and Long [6] who also performed experiments on the WGSR in the presence of H_2 at 1173 K and 1 atm. The shock-tube WGSR experiments in the presence of H_2 were performed at 290 and 194 atm with initial mole fractions of approximately 200 ppm of CO, 270 ppm of H_2O, and 300 ppm of H_2 as the dopant. Figures 7 and 8 show the 290 and 194 atm experiments, respectively, with H_2 now displayed in the plot. The reactivity trends are now changed with reduced CO reaction (less than 10%), but do appear to exhibit the same overall qualitative trends as the experiments that did not include H_2 as a reactant, with the onset of reaction at $T > 1600$ K. The observed reaction is small and the CO profile, and correspondingly CO_2, attains a plateau at $T > 1800$ K. It is evident that H_2, a product in the WGSR, affects the equilibrium and, consequently, the plateau or quasi-equilibrium state observed in the reactant and product profiles occur with overall lesser reactivity. The H_2 was used as a reactant to compare to Graven and Long's work, but CO_2 is a more abundant species in rocket exhaust and would have the same inhibiting effect on the overall reaction because it too is a product of the WGSR.

Discussion

The high-pressure experiments were simulated using the SENKIN module within the CHEMKIN [14] suite of programs. The simulations were performed using the constant pressure approximation. As a first step to simulate the experimental data, we have used a recently developed comprehensive CO oxidation model by Sivaramakrishnan et al. [13] consisting of 34 elementary reactions and 14 species. Other mechanisms, such as the GRI3.0[§] and the Li et al. model [15], were used to simulate our data, but neither fared better than the Sivaramakrishnan et al. [13] model. The comprehensive model has been validated against experiments on CO and H_2 combustion over a variety of experiments spanning a wide range of conditions, particularly high pressures, as in the current work, and thereby represents an ideal first choice model to simulate our experiments. Thermodynamic data have been obtained from this

[§]Smith, G. P., Golden, D. M., Frenklach, M., Moriarty, N. W., Eiteneer, B., Goldenberg, M., Bowman, C. T., Hanson, R. K., Song, S., Gardiner, W. C., Jr., Lissianski, V. V., and Qin, Z.; http://www.me.berkeley.edu/gri_mech [cited 10 August 2006].

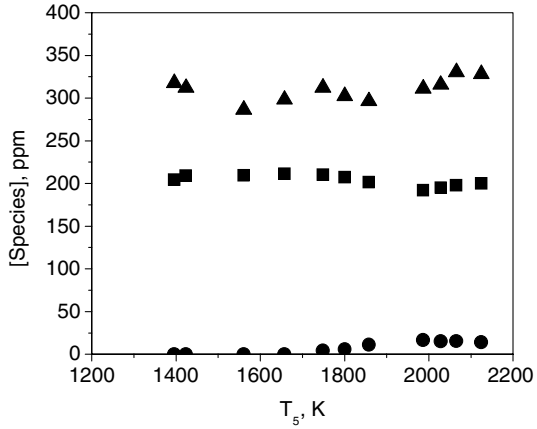

Fig. 7 290 atm, 200 ppm with H_2: ■ CO experiment, ● CO_2 experiment, ▲ H_2 experiment.

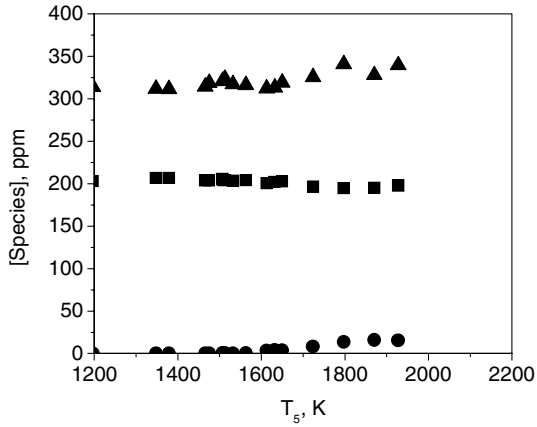

Fig. 8 194 atm, 200 ppm with H_2: ■ CO experiment, ● CO_2 experiment, ▲ H_2 experiment.

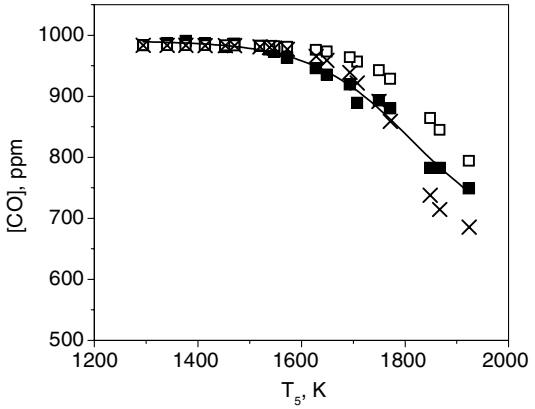

Fig. 9 307 atm, 1000 ppm model comparison: ■ CO experiment, □ CO model, X CO Bradford four-step mechanism. Solid line denotes experimental fit.

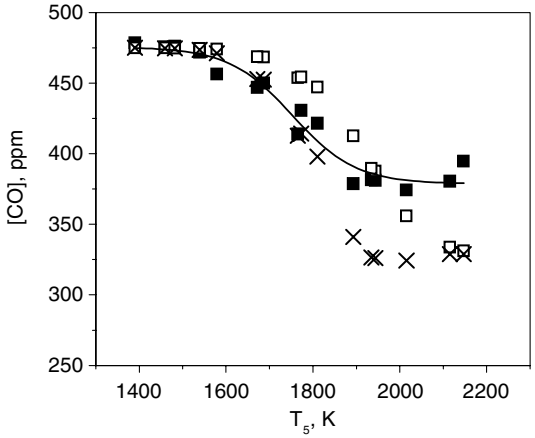

Fig. 10 299 atm, 475 ppm model comparison: ■ CO experiment, □ CO model, X CO Bradford four-step Mechanism. Solid line denotes experimental fit.

work [13] and recent recommendations [16] to ensure accurate thermodynamic values were used for each species in the simulations.

Figure 9 shows the CO predictions calculated from the comprehensive model for the 307 atm, 1000 ppm CO/H_2O experiments. The comprehensive model predicts an onset of CO reaction at $T > 1600$ K in contrast to the experiments showing reaction at $T > 1525$ K, with the model predictions trailing the observed experimental data at the higher temperatures with discrepancies being within 10% at the highest temperatures.

Figures 10 and 11, depicting the model predictions to the dilute reagent experiments (299 atm, 475 ppm and the 490 atm, 237.5 ppm), show trends that differ in their predictive capability with regard to the trends seen earlier in Fig. 9. The model predictions appear reasonable at the lower temperatures but, at the higher temperatures, the observed plateau in the CO experiments is not predicted by the model, with the model showing further CO consumption at $T > 2100$ K. In general, the model is able to make reasonable predictions of the data with the best fit obtained for the data set with larger initial concentrations of the reactants.

To determine which reactions dominate the CO consumption in the comprehensive model, a sensitivity analysis for CO was performed for the 300 and 500 atm experiments at 1770 K and 1.1 ms. The simulations revealed only four reactions among the 34 of the comprehensive model showing CO sensitivity. Bradford [8] has previously postulated a simplified four-step mechanism for the WGSR that consists of three of the four sensitive reactions from the comprehensive model. The mechanism involves a chain initiation reaction [reaction (4)], followed by two propagation reactions (5) and (6), and reaction (7) [the reverse of reaction (4)], the termination step:

$$H_2O + M \xrightarrow{k_4} H + OH + M \tag{4}$$

$$CO + OH \underset{k_{-5}}{\overset{k_5}{\Leftrightarrow}} H + CO_2 \tag{5}$$

$$H_2O + H \underset{k_{-6}}{\overset{k_6}{\Leftrightarrow}} OH + H_2 \tag{6}$$

$$H + OH + M \xrightarrow{k_{-4}} M + H_2O \tag{7}$$

$$CO + H_2O \overset{k}{\Leftrightarrow} CO_2 + H_2 \tag{8}$$

Reaction (8) thus represents the overall WGSR that is obtained by a summation of reactions (4–7). Applying a steady-state analysis and neglecting reverse reactions, the overall rate for CO_2 formation or, alternately, CO consumption is given by

$$r = -\frac{d[CO]}{dt} = \frac{d[CO_2]}{dt} = \left[\frac{k_4}{k_{-4}} k_5 k_6\right]^{0.5} [CO]^{0.5}[H_2O] = k[CO]^{0.5}[H_2O] \tag{9}$$

where $-r$ is the global rate of CO_2 formation and k is the global rate coefficient for CO_2 formation.

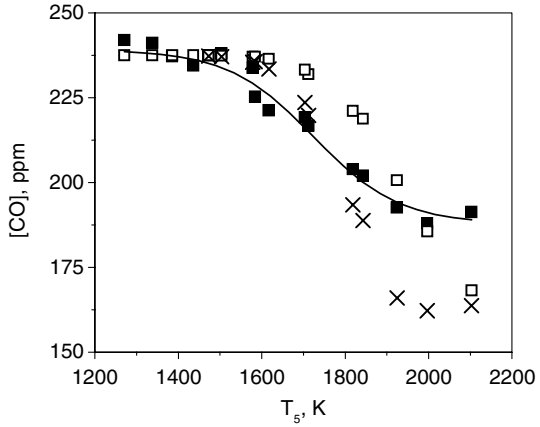

Fig. 11 490 atm, 237.5 ppm model comparison: ■ CO experiment, □ CO model, X CO Bradford four-step Mechanism. Solid line denotes experimental fit.

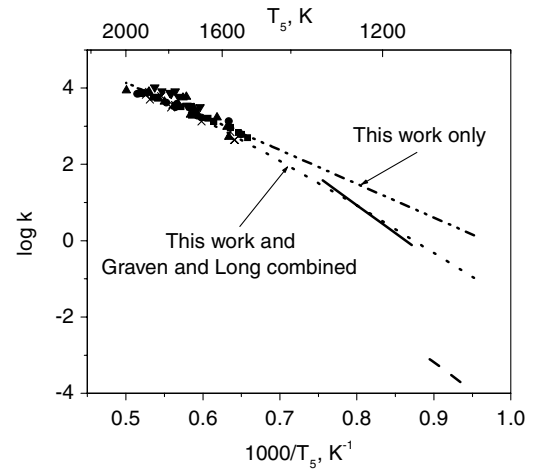

Fig. 12 Rate constant comparison: solid line, Graven and Long (1 atm) [6]; dashed line, Bustamante et al. (16 atm) [2,3]; dash-dots-dash line, fit to this work only; dotted line, non-Arrhenius fit to this work and Graven and Long [6]; ■ 307 atm, 1000 ppm; ● 299 atm, 475 ppm; ▲ 490 atm, 237.5 ppm; ▼ 296 atm, 120.7 ppm; X 475 atm, 115 ppm. Units of k are $[(\mathrm{L/mol})^{0.5}\mathrm{s}^{-1}]$.

The overall reaction rate coefficient for CO_2 formation or, alternately, CO consumption is calculated using the derived Eq. (9) and the measured initial and final concentrations of the reactants and products, along with the reaction time of each shock at each corresponding shock temperature. Because each experiment had approximately the same reaction time of 1 ms, the quantity $\mathrm{d}[CO_2]/\mathrm{d}t$ is largely dependant on the change in CO_2, which changes due to reaction temperature. Because our measurement technique does not track the time history of the products, the quantity $\mathrm{d}[CO_2]/\mathrm{d}t$ is determined as $\Delta[CO_2]/\Delta t$. A typical Arrhenius plot depicting the logarithm of the global rate coefficient against temperature is shown in Fig. 12. At higher temperatures above 2000 K, when the CO profiles plateau, it will be shown later that the reaction has reached equilibrium. Because the higher temperature experiments were at or near equilibrium at the end of the reaction time, it would be incorrect to include them in the Arrhenius plot and they were therefore omitted. The symbols in the figure represent the derived rate coefficients from the HPST experimental data (Figs. 1–5) using Eq. (9). It is seen from this figure that the current experimental data corroborate the Graven and Long [6] rate equation, and the derived rate coefficients lie in a tight narrow band, further demonstrating the one-half order dependence on CO that was found in the literature and derived in Eq. (9). The Graven and Long [6] and Bustamante et al. [2,3] suggested rate parameters are plotted over their respective experimental temperatures. One other feature to note in this plot is that the rate coefficients derived from the higher pressure (1.6 MPa) results of Bustamante et al. [3] are less than the current data sets at much higher pressures, as well as the 1 atm data sets of Graven and Long [6]. However, Bustamante et al. [3] mention in their article that they observe no pressure dependency between their 0.1 and 1.6 MPa experiments, which appears to contradict the rate coefficients derived from their experiments.

Overall, Fig. 12 shows that the global WGSR rate coefficient calculated using only our high-pressure, high-temperature experiments (denoted by the dash-dot-dash line) extrapolated to the lower temperature regime of Graven and Long [6] varies from a factor of 2 at their highest temperatures (1325 K) to as much as an order of magnitude at their lowest temperatures (1150 K). The rate expression suggested by Graven and Long is represented in Eq. (10), which was suggested for use at lower temperatures of 1150–1325 K:

$$\frac{\mathrm{d}[CO_2]}{\mathrm{d}t} = 5.0 \times 10^{12} \exp\left(-\frac{67300}{RT}\right)[CO]^{0.5}[H_2O] \qquad (10)$$

where E_a is in units of cal/mol, the preexponential factor is in units of $(\mathrm{L/mol})^{1/2}\mathrm{s}^{-1}$, and the concentrations are in units of mol/L.

Because extrapolating the Arrhenius fit of our high-temperature, high-pressure data down to the temperature regime of Graven and Long [6] does not match the Graven and Long values, a three parameter non-Arrhenius fit (denoted with a dotted line) was determined, which matches both our high-temperature data, as well as that from Graven and Long at lower temperatures, and is shown in Eq. (11). Though the experimental temperatures do not quite reach the extreme levels observed in rocket motors, these higher temperature experiments were crucial in discovering a temperature dependence that was not observed before:

$$\frac{\mathrm{d}[CO_2]}{\mathrm{d}t} = 7.7 \times 10^{45}\ T^{-10} \exp\left(-\frac{80,000}{RT}\right)[CO]^{0.5}[H_2O] \qquad (11)$$

The analysis for the experiments in which H_2 was added as a dopant (Figs. 7 and 8) involves an additional parameter when evaluating the rate coefficient due to H_2 dissociation becoming important:

$$\mathrm{H} + \mathrm{H} + \mathrm{M} \underset{k_{-12}}{\overset{k_{12}}{\Leftrightarrow}} \mathrm{H_2} + \mathrm{M} \qquad (12)$$

When reaction (12) is added to the chemistry, the overall reaction rate expression is modified by the H_2 concentration and is represented by Eq. (13), as suggested by Graven and Long [6]. Equation (13) also incorporates the Graven and Long rate parameters and their fitting parameter B:

$$\frac{\mathrm{d}[CO_2]}{\mathrm{d}t} = k\frac{[CO]^{0.5}[H_2O]}{(1 + \mathrm{B}[H_2])^{0.5}} = 5.0 \times 10^{12} \exp\left(-\frac{67,300}{RT}\right)\frac{[CO]^{0.5}[H_2O]}{(1 + 1.2 \times 10^4[H_2])^{0.5}} \qquad (13)$$

Using our HPST experiments not containing H_2 to obtain the rate in Eq. (11), the experiments with H_2 were used to modify this fitting parameter B that accounts for the H_2 concentrations in the reactant mixture and is displayed in Eq. (14):

$$\frac{\mathrm{d}[CO_2]}{\mathrm{d}t} = k\frac{[CO]^{0.5}[H_2O]}{(1 + \mathrm{B}[H_2])^{0.5}} = 7.7 \times 10^{45}\ T^{-10} \exp\left(-\frac{80,000}{RT}\right)\frac{[CO]^{0.5}[H_2O]}{(1 + 3.7 \times 10^3[H_2])^{0.5}} \qquad (14)$$

The shock-tube experimental measurements have been used to evaluate the rate coefficient and the rate parameters using the rate expression in Eq. (14). Figure 13 depicts the derived HPST rate coefficients, the Graven and Long [6] rate coefficient at 1190 K represented by the cross, and the non-Arrhenius fit to these rate coefficients from this work and Graven and Long shown as the solid

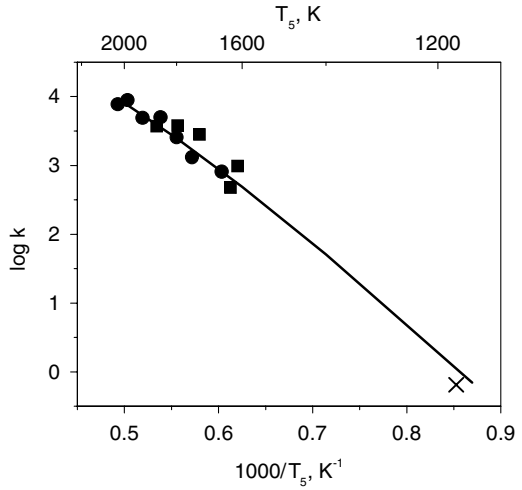

Fig. 13 Rate constant comparison for mixture with H_2: ● 290 atm, 200 ppm; ■ 194 atm, 200 ppm; X Graven and Long experiment [6]; solid line non-Arrhenius fit to this work and Graven and Long. Units of k are $[(L/mol)^{0.5}s^{-1}]$.

line. The non-Arrhenius three-parameter fit provides a close match to these HPST coefficients, as well as the lower temperature Graven and Long rate coefficients.

Model Modifications

Preliminary simulations with the comprehensive model [13] indicated a satisfactory match to the experimental reactivity trends. To better predict the present HPST results, we have attempted to probe the existing comprehensive model and develop a simplified four-step mechanism, akin to the Bradford mechanism [8], although with updated rate coefficients. The sensitivity analyses previously mentioned, now shown in Fig. 14, depict that our assumption of the simple four-step Bradford mechanism is sufficient to provide an accurate description of the WGSR system. Figure 14 depicts the sensitivity analyses for the nominally 300 atm experiments at a characteristic $T = 1770$ K and a reaction time of 1.1 ms. CO concentrations are sensitive to only the four reaction steps in the Bradford mechanism:

$$H_2O + M \underset{k_{-4}}{\overset{k_4}{\Leftrightarrow}} H + OH + M$$

$$CO + OH \underset{k_{-5}}{\overset{k_5}{\Leftrightarrow}} H + CO_2$$

$$H_2O + H \underset{k_{-6}}{\overset{k_6}{\Leftrightarrow}} OH + H_2$$

$$H + H + M \underset{k_{-12}}{\overset{k_{12}}{\Leftrightarrow}} H_2 + M$$

We have analyzed the rate coefficients for the three reactions (4–6). Reaction (12) H_2 dissociation is at its low-pressure limit and its rate coefficient is fairly well characterized and, furthermore, CO concentrations exhibit negligible sensitivity to this reaction. The rate

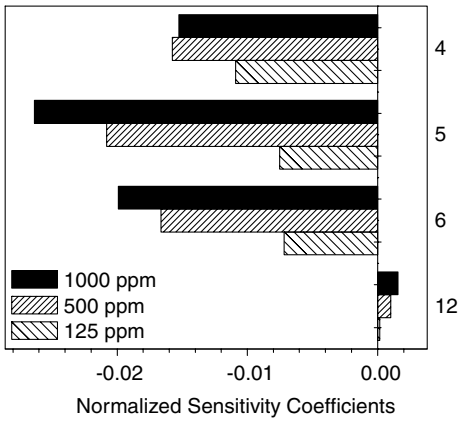

Fig. 14 Normalized sensitivity coefficients for CO at 300 atm, 1770 K, and 0.0011 s reaction time.

coefficient for reaction (6) appears to be well characterized for a wide range of temperatures and pressures as shown in the work by Michael and Sutherland [17], as well as in the Baulch et al. [18] review, which quotes a small uncertainty for this reaction. The only two other reactions of importance in this system are reaction (4), the water dissociation reaction, and reaction (5), the bimolecular reaction between CO and OH. Reaction (5) plays the dominant role in CO consumption under the conditions of the present experiments. This reaction, despite the high-pressure conditions in this work, remains a bimolecular channel with the elevated temperatures ruling out the possibility of the stabilized HOCO adduct [19]. This reaction has been studied at high pressures by Fulle et al. [20], Wooldridge et al. [21], and in the comprehensive model [13], where the rate coefficients for this reaction were optimized against a variety of targets. To test the sensitivity of this channel, we replaced these optimized rate coefficients with the direct experimental measurements of Fulle et al. [20] which span a high-pressure regime in the assembled four-step model.

Next, reaction (4) was investigated. There have been recent experimental results by Srinivasan and Michael [22] that show H_2O decomposition is faster than previously thought. The Baulch et al. [18] review also quotes a fairly large uncertainty for the rate coefficients for this reaction at high temperatures. Both the recommended rate coefficients by Srinivasan and Michael [22], on the basis of their experiments and other experiments spanning a wide temperature range, as well as their direct experimental high-temperature rate coefficients, were used in the four-step model. A modified value of the experimental rate coefficient, shown in Table 2, provided the best fit to the experimental data. Using this set of rate coefficients in the four-step reaction (Table 2) provided an improvement over the comprehensive model's [13] predictions of our experimental data.

Figures 9–11 compare the four-step mechanism to the comprehensive model and the experimental CO concentrations. It can be seen that the four-step model is better at capturing the temperature at which CO begins to react. Furthermore, the updated four-step model is able to qualitatively predict the shape of the CO profile. The experimental CO profile attains a plateau at the higher temperatures, which is captured qualitatively well by the model (Figs. 10 and 11), albeit it predicts a larger rate of CO decrease. The

Table 2 Reaction rates for Bradford four-step method

	Reaction	A[a]	n	E_a[b]	Reference
4	$H_2O(+M) = OH + H(+M)$	1.464E14	0	93,621	[22]
5	$CO + OH = CO_2 + H$	1.084E13	0	3670	[20]
		9.637E11	0	268.2	
6	$OH + H_2 = H_2O + H$	2.167E8	1.51	3430	[17]
12	$H + H(+M) = H_2(+M)$	1.780E18	−1	0	[13]

[a]A: $cm^3\ mol^{-1}\ s^{-1}$.
[b]E_a: $cal\ mol^{-1}$.

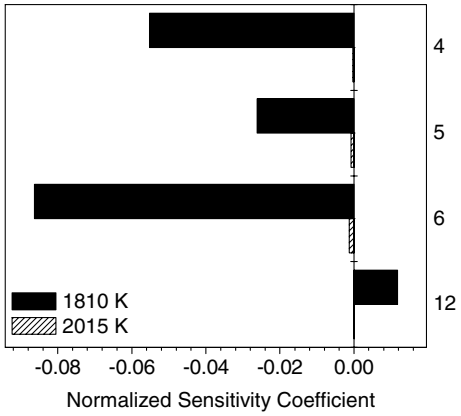

Fig. 15 Normalized sensitivity coefficients for CO at 299 atm, 475 ppm, and 0.0011 s reaction time.

improvement only results from the two new rate coefficients implemented into the four-step model. If the particular rate constants from the GRI3.0 database (see footnote [§] on p. 1087) were applied to the four-step mechanism, the CO profile would lie right on top of the original comprehensive model CO profile in Figs. 9–11.

A sensitivity study was performed on the four-step model for CO consumption at 299 atm, 475 ppm, 1.1 ms and two different temperatures, one in which CO was reacting (1810 K) and one in which the CO had leveled off (2015 K). Figure 15 compares the normalized sensitivities for the two temperatures for each reaction. As shown in Fig. 15, the reactions that CO was sensitive to become insignificant, which explains the leveling off of CO and illustrates that the reaction has reached equilibrium in the higher temperature experiments.

Overall, the comprehensive model does a satisfactory job predicting the CO concentration, but the four-step model provides a better fit to the experimental data. However, one should note that this four-step model is only applicable for the WGSR, whereas the comprehensive model can accurately predict the combustion of H_2/CO mixtures over wide temperature and pressure ranges [13]. The four-step mechanism is limited to simulating WGSR because it lacks most of the chemistry necessary to simulate the full H_2/CO combustion chemistry.

Conclusions

The WGSR was experimentally probed at elevated temperatures and pressures that more closely reflect the conditions existent in the postcombustion zone of the rocket nozzle than previous data. The experimental data were used to obtain a global rate coefficient for CO_2 formation. The current study appears to be the only thermal investigation on the WGSR under such elevated conditions and therefore represents a better estimate of the global WGSR rate coefficient for the rocket nozzle environment. The present experimental study in the high-pressure shock tube illustrates that the global reaction rate coefficient is

$$\frac{\mathrm{d}[CO_2]}{\mathrm{d}t} = 7.7 \times 10^{45}\ T^{-10} \exp\left(-\frac{80,000}{RT}\right)[CO]^{0.5}[H_2O]$$

The derived rate coefficients match fairly well the lower temperature 1 atm flow reactor measurements reported in the literature [6]. For the purpose of this project, the investigation of rocket nozzle erosion due to heterogeneous chemistry at elevated pressures, the overall WGSR rate coefficient was found to be independent of pressure.

Acknowledgments

This research is supported by subcontract 2799-UI-ONR-0683 from the Pennsylvania State University through the U.S. Office of Naval Research Multidisciplinary University Research Initiative (prime award N0014-04-1-0683) under the direction of Ken Kuo.

References

[1] Kuo, K. K., and Keswani, S. T., "Comprehensive Theoretical Model for Carbon-Carbon Composite Nozzle Recession," *Combustion Science and Technology*, Vol. 42, Nos. 3–4, 1985, pp. 145–164. doi:10.1080/00102208508960374

[2] Bustamante, F., Enick, R. M., Cugini, A. V., Killmeyer, R. P., Howard, B. H., Rothenberger, K. S., Ciocco, M. V., Morreale, B. D., Chattopadhyay, S., and Shi, S., "High-Temperature Kinetics of the Homogeneous Reverse Water-Gas Shift Reaction," *AIChE Journal*, Vol. 50, No. 5, 2004, pp. 1028–1041. doi:10.1002/aic.10099

[3] Bustamante, F., Enick, R. M., Killmeyer, R. P., Howard, B. H., Rothenberger, K. S., Cugini, A. V., Morreale, B. D., and Ciocco, A. V., "Uncatalyzed and Wall-Catalyzed Forward Water-Gas Shift Reaction Kinetics," *AIChE Journal*, Vol. 51, No. 5, 2005, pp. 1440–1454. doi:10.1002/aic.10396

[4] Keiski, R. L., Salmi, T., Niemistoe, P., Ainassaari, J., and Pohjola, V. J., "Stationary and Transient Kinetics of the High Temperature Water-Gas Shift Reaction," *Applied Catalysis, A: General*, Vol. 137, No. 2, 1996, pp. 349–370. doi:10.1016/0926-860X(95)00315-0

[5] Van der Laan, G. P., and Beenackers, A. A. C. M., "Kinetics and Selectivity of the Fischer-Tropsch Synthesis: A Literature Review," *Catalysis Reviews: Science and Engineering*, Vol. 41, Nos. 3–4, 1999, pp. 255–318. doi:10.1081/CR-100101170

[6] Graven, W. M., and Long, F. J., "Kinetics and Mechanisms of the Two Opposing Reactions of the Equilibrium $CO + H_2O = CO_2 + H_2$," *Journal of the American Chemical Society*, Vol. 76, No. 10, 1954, pp. 2602–2607. doi:10.1021/ja01639a002

[7] Hadman, G., Hinshelwood, C., and Thompson, H., "Oxidation of Carbon Monoxide," *Proceedings of the Royal Society of London*, Vol. 137, No. 831, 1932, pp. 87–101. doi:10.1098/rspa.1932.0123

[8] Bradford, B. W., "Water-Gas Reaction in Low-Pressure Explosions," *Journal of the Chemical Society*, Pt. 2, 1933, pp. 1557–1563. doi:10.1039/jr9330001557

[9] Long, F. J., and Sykes, K. W., "Catalysis of the Carbon Monoxide-Steam Reaction," *Proceedings of the Royal Society of London A*, Vol. 215, No. 1120, Nov. 1952, pp. 111–119.

[10] Tranter, R. S., Brezinsky, K., and Fulle, D., "Design of a High-Pressure Single Pulse Shock Tube for Chemical Kinetic Investigation," *Review of Scientific Instruments*, Vol. 72, No. 7, 2001, pp. 3046–3054. doi:10.1063/1.1379963

[11] Tranter, R. S., Sivaramakrishnan, R., Srinivasan, N., and Brezinsky, K., "Calibration of Reaction Temperatures in a Very High Pressure Shock Tube Using Chemical Thermometers," *International Journal of Chemical Kinetics*, Vol. 33, No. 11, 2001, pp. 722–731. doi:10.1002/kin.1069

[12] Tang, W., and Brezinsky, K., "Chemical Kinetic Simulations Behind Reflected Shock Waves," *International Journal of Chemical Kinetics*, Vol. 38, No. 2, 2006, pp. 75–97. doi:10.1002/kin.20134

[13] Sivaramakrishnan, R., Comandini, A., Tranter, R. S., Davis, S. G., Wang, H., and Brezinsky, K., "Combustion of CO/H2 Mixtures at Elevated Pressures," *Proceedings of the Combustion Institute*, Vol. 31, No. 1, 2007, pp. 429–437. doi:10.1016/j.proci.2006.08.057

[14] Kee, R. J., Rupley, F. M., Miller, J. A., Coltrin, M. E., Grcar, J. F., Meeks, E., Moffat, H. K., Lutz, A. E., Dixon-Lewis, G., Smooke, M. D., Warnatz, J., Evans, G. H., Larson, R. S., Mitchell, R. E., Petzold, L. R., Reynolds, W. C., Caracotsios, M., Stewart, W. E., Glarborg, P., Wang, C., and Adignun, O., CHEMKIN Collection, Release 3.6 ed., Reaction Design, San Diego, CA, 2000.

[15] Li, J., Zhao, Z., Kazakov, A., and Dryer, F. L., "Updated Comprehensive Kinetic Model of Hydrogen Combustion," *International Journal of Chemical Kinetics*, Vol. 36, No. 10, 2004, pp. 566–575. doi:10.1002/kin.20026

[16] Burcat, A., and Ruscic, B., "Third Millennium Thermodynamic Database for Combustion and Air-Pollution Use with Updates from Active Thermochemical Tables," Repts. ANL 05-20 and TAE 960, Sept. 2005; ftp://ftp.technion.ac.il/pub/supported/aetdd/thermodynamics [cited 15 Oct. 2006].

[17] Michael, J. V., and Sutherland, J. W., "Rate Constants for the Reaction of Hydrogen Atom with Water and Hydroxyl with Hydrogen by the Flash Photolysis-Shock Tube Technique over the Temperature Range 1246–2297 K," *Journal of Physical Chemistry*, Vol. 92, No. 13, 1988, pp. 3853–3857. doi:10.1021/j100324a035

[18] Baulch, D. L., Bowman, C. T., Cobos, C. J., Cox, R. A., Just, Th., Kerr, J. A., Philling, M. J., Stocker, D., Troe, J., Tsang, W., Walker, R. W., and Warnatz, J., "Evaluated Kinetic Data for Combustion Modelling: Supplement 2," *Journal of Physical and Chemical Reference Data*, Vol. 34, No. 3, 2005, pp. 757–1397. doi:10.1063/1.1748524

[19] Joshi, A. V., and Wang, H., "Master Equation Modeling of Wide Temperature and Pressure Dependence of $CO + OH \rightarrow$ Products," *International Journal of Chemical Kinetics*, Vol. 38, No. 1, 2006, pp. 57–73. doi:10.1002/kin.20137

[20] Fulle, D., Hamann, H. F., Hippler, H., and Troe, J., "High Pressure Range of Addition Reactions of HO, 2: Temperature and Pressure Dependence of the Reaction $HO + CO \Leftrightarrow HOCO \rightarrow H + CO_2$," *Journal of Chemical Physics*, Vol. 105, No. 3, 1996, pp. 983–1000. doi:10.1063/1.471991

[21] Wooldridge, M. S., Hanson, R. K., and Bowman, C. T., "Shock Tube Study of the $CO + OH \rightarrow CO_2 + H$ Reaction," *Proceedings of the Combustion Institute*, Vol. 25, 1994, pp. 741–748.

[22] Srinivasan, N. K., and Michael, J. V., "Thermal Decomposition of Water," *International Journal of Chemical Kinetics*, Vol. 38, No. 3, 2006, pp. 211–219. doi:10.1002/kin.20172

V. Yang
Editor-in-Chief